Journal of Control, Automation and Electrical Systems (2022) 33:1217–1228
https://doi.org/10.1007/s40313-021-00881-z

Ultra-local Model Design Based on Real-time Algebraic and Derivative Estimators for Position Control of a DC Motor

Laid Sehili[1] · **Boubekeur Boukhezzar**[1]

Received: 23 June 2021 / Revised: 4 November 2021 / Accepted: 30 November 2021 / Published online: 3 January 2022

Abstract
This paper intends to study and implement recent state observation techniques of the ultra-local model used in model-free control approach in two different methodologies, through an ultra-local model-based algebraic estimator and using an ultra-local model-based derivative estimator. The estimation is based on Taylor's expansion coefficients for an arbitrary order. This research serves a discrete implementation details of the proposed approach using operational calculus and finite impulse response filters. A comparative study between algebraic and derivative estimators is presented. Different tests have been verified on a position trajectory control scheme of a DC motor that is subjected to disturbances and uncertainties. The used ultra-local model design is independent of initial conditions and stands in need only to measure the system's input and output values. This study shows that the proposed design reduces the nonlinearities and increases the robustness to disturbances resulting from Coulomb friction effects. Moreover, the algebraic and derivative estimation process is computed in real-time. The evidence of the recommended approaches has been examined by numerical simulation and compared with other strategies.

Keywords Algebraic estimator · Derivative estimator · Model-free control · Disturbance rejection · DC motors · Intelligent PID

1 Introduction

DC motors have been commonly used in industries along with their impressive speed control characteristics, even though their operating costs are higher than the induction motor (Lyshevski 1999). Consequently, the DC motor's position control has acquired substantial studies where many techniques have been developed. Its key benefit is that speed or positioning control is easily adaptable for an extensive range to track a default time trajectory in response to various load inputs. In the past, numerous researches have been conducted, and literature covers many applications: motion control of a disk (Yavin 2007), overhead cranes control (Mahfouf et al. 2000), liquid pumps (Mummadi 2000), wheeled mobile manipulator (Tang et al. 2010), positioning tables (Wang et al. 2011). In that cases, Coulomb frictions and unmodeled dynamics have to be considered. Recently, researchers have shown an increased interest in studying appropriate control techniques that utilize high-precision and high-speed tracking functionality of DC motors. Time response is typically essential for high efficiency, and precision/exactness becomes increasingly stringent as modern electromechanical applications have a reduced size. High speed is generally necessary to obtain an increased productivity, and accuracy is increasingly stringent due to the small size of current electromechanical systems (Ruderman et al. 2020). Eker (2004) integrated the usual discrete time algorithms with root mean square errors to identify and control the mechanical systems. Nouri et al. (2008) examined the issue of speed regulation through recurring neural networks and introduced a sliding mode control with a PID type sliding surface (Eker 2006). Mamani et al. (2007, 2009) conducted a classical control technique using the system model which is known frequently, and used an adaptive control approach to improve the control performance. An other adaptive control approach was designed using bacterial foraging algorithm (Bhushan and Singh 2011). Guermouche et al. (2015) controlled the DC motor position via disturbance observer. A

✉ Laid Sehili
laid.sehili@umc.edu.dz

Boubekeur Boukhezzar
boubekeur.boukhezzar@umc.edu.dz

[1] Laboratory of Automation and Robotics (LARC), Faculty of Technology, Frères Mentouri Constantine 1 University, Constantine 25000, Algeria

study by Aravind et al. (2017) examined an optimization technique with LQG controller.

Preliminary work on algebraic techniques for rapid online and accurate identification or estimation of system parameters, failures, states, and input perturbations have been established in recent years in the studies of Fliess and Sira-Ramírez. The principles of the technique for linear systems case study was reported by Fliess and Sira-Ramirez (2003) where one of the parameter identifiers for the model of the DC motor has been outlined by Mamani et al. (2007). Fliess and Join (2013) introduced the model-free control approach (MFC) which expands the classical PID controllers and sets "intelligent" PID controllers (iPID) that contribute to the system's unknown dynamics and can be used to enhance the reference tracking. Since MFC does not require a nominal model, the control methodology is implicitly robust. Much successful research is being processed using MFC: vehicles system control (Polack et al. 2019), magnetic levitation systems (Moraes and da Silva 2015), quadrotor helicopters (Glida et al. 2020), fuel power generation (Mungporn et al. 2019), hybrid unmanned aerial vehicles (Barth et al. 2019), exoskeleton-upper limb system (Bembli et al. 2021), and other applications.

In this paper, model-free control technique is proposed based on an ultra-local combined with simultaneous implementation of algebraic and derivative estimators. In previous studies, the estimation techniques were based on ALIEN filters (Fliess and Join 2013), and this work relies on FIR filters. Moreover, a clear and quick tuning algorithm of the ultra-local model parameter is proposed.

It is important to note that the used DC motor in this research is subjected to Coulomb friction effects and have un-modeled dynamics. Therefore, this study contributes to existing knowledge of DC motors position control that are subjected to internal and external disturbances. In a first point of view, nonlinear controllers have more attractive features than linear controllers in terms of the tracking error to be minimized along with the trajectory tracking; simultaneously, the proposed algebraic/derivative approaches can ensure better control law with a quick, non-asymptotic, and accurate state estimation. Besides showing the closed-loop control estimators' efficiency, the research also offers important insights and simplifies several aspects of a detailed digital implementation of these modern controllers.

This paper has been divided into the following sections: Sect. 2 illustrates the DC motor's dynamic model and the problem formulation. Section 3 gives a brief overview of the ultra-local model and model-free control, the used estimation techniques and their implementations, and the controller design procedure. In Sect. 4, the findings of the research are presented. Finally, the conclusion gives a brief summary and critique of the findings.

Table 1 Parameters of the DC motor

Variable	Value
k (N· m / V)	0.21
J (kg· m^2)	6.87×10^{-5}
v (N· m· s)	1.041×10^{-3}
n	50

2 DC Motor Model and Problem Formulation

2.1 DC Motor Dynamics

The context of the used linear model for the DC motor is covered in this section. This linear model is considered to be affected by an uncertain disturbance input and Coulomb friction effects (Olsson et al. 1998). The basic dynamic equation of the system is derived from Newton's second law:

$$kV = J\ddot{\hat{\theta}}_m + v\dot{\hat{\theta}}_m + \hat{\Gamma}_c(\dot{\hat{\theta}}_m) \tag{1}$$

where V is the DC motor input voltage fed to the system as a control variable signal, the magnitude of J is the motor's gear inertia (kg · m^2), v is the coefficient of viscous friction (N· m· s), k is the electromechanical constant (N · m / V), and $\hat{\Gamma}_c$ is the torque of the unknown friction that impacts the motor dynamics. The nonlinear term of the friction is viewed as a disturbance and describes the following equation:

$$\hat{\Gamma}_c = \hat{\Gamma}_{Coul} sign(\dot{\hat{\theta}}_m) \tag{2}$$

where $\hat{\Gamma}_{Coul}$ is the static friction value that must surpass the rotational velocity in order to start rotating around the vertical axis. The terms $\ddot{\hat{\theta}}_m$, $\dot{\hat{\theta}}_m$ and $\dot{\hat{\theta}}_m$ are used to refer to the angular acceleration (rad/s^2), angular velocity (rad/s) and angular position (rad) of the motor, respectively. The constant parameter n is the motor gear reduction factor. Hence, $\theta_m = \hat{\theta}_m/n$, where θ_m is the motor's gear position and $\hat{\theta}_m$ is the motor shaft's position. Furthermore, $\Gamma_c = \hat{\Gamma}_c/n$, where Γ_c is the motor gear's Coulomb friction torque.

The type of the used DC motor in simulations is: RH-8D-6006-E036AL-SP(N) (Mamani et al. 2009), where the shaft may turn across the vertical axis, either left or right. See the description of the parameters in Table 1.

2.2 Problem Formulation

Consider the DC motor dynamics discussed above in (1). Provided that the reference path θ_m^*(t) is properly smooth for the trajectory tracking of the DC motor, and considering so-called signal input noises, V, and of the output, θ_m(t), in addition to the existence of unknown nonlinear effects resulting from model parametric uncertainties or Coulomb friction

effects, the feedback controller must accomplish precisely the asymptotic tracking of $\theta_m^*(t)$ through the system output $\theta_m(t)$.

3 Model-free Control Approach

3.1 General Principle

Consider a system in which the output is y, and the input is u. If $\mathfrak{S}$ is not necessarily linear but an essentially smooth function, the differentiation equation between the input and output can be represented as in (3) (Mboup et al. 2007):

$$\mathfrak{S}\left(t, u, \dot{u}, \ldots, u^{(m)}, y, \dot{y}, \ldots, y^{(n)}\right) = 0 \tag{3}$$

If there exist $i \in]0; n[$ such that $\frac{\partial \mathfrak{S}}{\partial y^{(i)}} \neq 0$, then the absolute function theorem returns locally to:

$$y^{(i)} = \mathfrak{S}\left(t, u, \dot{u}, ..., u^{(m)}, y, \dot{y}, ..., y^{(i-1)}, y^{(i+1)}, ..., y^{(n)}\right) \tag{4}$$

3.2 Ultra-local Model

The theory of model-free control technique developed by Fliess and Join (2013) is to substitute an ultra-local model given by the complex nonlinear model in (4) such that:

$$y^{(v)}(t) = F(t) + \beta u(t) \tag{5}$$

where

- $y^{(v)}$ is the v-order derivative of the observed output. v is a positive integer picked by practice and may be chosen to be 1, or rarely 2. It is selected to be equal to 1 in the rest of this research for better transient performance.
- F represents the un-modeled dynamics of the plant, including the unexpected disturbances. This piece-wise constant function is continuously updated and identified in real-time via algebraic approaches (Fliess and Sira-Ramirez 2003). The determination of F through derivative estimation is another possible estimation technique (Mboup et al. 2007).
- $\beta \in \mathbb{R}$ is a non-physical parameter selected by the designer such that βu and $y^{(v)}$ are of the same sign and magnitude. By testing, until a perfect closed-loop performance is acquired, this choice is obtained.

In a short time interval, the ultra-local model is seen as an approximate dynamic. This model is used for the control synthesis. It allows the nonlinear mathematical system modeling to be omitted from the complex task and contributes to precise gain tuning.

Consider the ultra-local model in (5) once more, then closing the loop through an intelligent PID controller:

$$F(t) = y^{(v)}(t) - \beta u(t) \tag{6}$$

The control signal can be represented as follows:

$$u = -\frac{F - y_d^{(v)} + u_C}{\beta} \tag{7}$$

where

- $y_d^{(v)}$ is the v^{th} derivative of the output reference trajectory.
- u_c is a causal feedback control signal.

Combining (6) and (7) yields:

$$y^{(v)} = F + \beta\left(-\frac{F - y_d^{(v)} + u_c}{\beta}\right) = y_d^{(v)} - u_c \tag{8}$$

Afterward,

$$y^{(v)} - y_d^{(v)} + u_c = 0 \tag{9}$$

$$e^{(v)} + u_c = 0 \tag{10}$$

where $e^{(v)}$ is the v^{th} derivative error of $(e = y - y_d)$. u_c should be chosen to ensure a perfect asymptotic tacking where the output converges to the reference trajectory, i.e.,

$$\lim_{t \to +\infty} e(t) = 0 \tag{11}$$

3.3 Intelligent PIDs (iPIDs)

Set the control signal in (7) with a classic PID controller,

$$u = -\frac{F - \ddot{y}_d + K_P e + K_I \int e + K_D \dot{e}}{\beta} \tag{12}$$

where $v = 2$ in (5). The intelligent proportional-integral-derivative controller (iPID) can be defined by substituting (5) in (12), that being so:

$$\ddot{e} + K_P e + K_I \int e + K_D \dot{e} = 0 \tag{13}$$

where F no longer shows up, i.e., the uncertainties and unmodeled plant dynamics are excluded. Equation (13) then readily fulfills the tracking requirements by means of a suitable tuning of the gains $\{K_P, K_I, K_D\}$. It results in a linear differential equation stability with real constant coefficients.

If $\{K_P \neq 0, K_I = 0, K_D = 0\}$, $\{K_P \neq 0, K_I = 0, K_D \neq 0\}$, $\{K_P \neq 0, K_I \neq 0, K_D \neq 0\}$, we obtain an intelligent Proportional (iP), intelligent Proportional-Derivative (iPD) and intelligent Proportional-Integral-Derivative (iPID) controllers respectively.

4 Online Estimation of the Ultra-local Model

The identification of the parameter F may be found using algebraic estimation (Fliess et al. 2008). The other proposed technique is the numerical differentiation known as a derivative estimation.

4.1 Identification Through Algebraic Estimation (Alg)

Consider equation (5). The classic principles of operational calculus are used in order to cover all preceding equations, where F is substituted by F_{approx} and presumed to remain constant over the interval $[t, t+T]$ and obtained by the following steps:

1. For $v = 1$ in (5), take the Laplace transformation:

$$sY(s) - y(0) = \frac{F_{\text{approx}}}{s} + \beta \mathrm{U(s)} \tag{14}$$

2. Differentiate (14) with respect to s to eliminate the initial condition $y(0)$:

$$Y(s) - s\frac{d}{ds}Y(s) = -s^{-2}F_{\text{approx}} + \beta\frac{d}{ds}\mathrm{U(s)} \tag{15}$$

3. Multiply both sides of (15) by $\frac{1}{s^2}$ (every component will be integrated at least once) to eliminate and filter the time derivatives to have a low-pass filter that attenuates noises:

$$\frac{1}{s^2}Y(s) + \frac{1}{s}\frac{d}{ds}Y(s) = -\frac{1}{s^{-4}}F_{\text{approx}} + \beta\frac{1}{s^3}\frac{d}{ds}U(s) \tag{16}$$

4. Note that the differentiation of $Y(s)$ with respect to s is associated with the multiplication by $-t$ in time domain, and the left multiplication of $Y(s)$ by $\frac{1}{s^\alpha}, \alpha \geq 1$ aligns with recursive integrals. In order to have a closed-form expression, the Cauchy formula for recurring integration is used for the operator $\frac{1}{s^\alpha}\frac{d^n}{ds^n}$ in just one integral:

$$\frac{1}{s^\alpha}\frac{d^n}{ds^n}Y(s) \longleftrightarrow \frac{(-1)^n}{(\alpha-1)!}\int_0^t (t-\tau)^{\alpha-1}\tau^n y(\tau)\mathrm{d}\tau \tag{17}$$

5. The corresponding estimated time domain expression of (16) will be:

$$F_{\text{approx}} = \frac{-6}{t^3}\int_0^t (t-2\tau)y(\tau)d\tau - \frac{6\beta}{t^3}\int_0^t \tau(t-\tau)u(\tau)d\tau \tag{18}$$

4.2 Identification Through Derivative Estimation (Der)

The second approach for estimating the parameter F in (5) is the identification through derivative estimation of the output signal $\dot{y}$ in (6).

The derivative estimation approach is identified based on the coefficients of Taylor expansion in an arbitrary order. The signal $\tilde{y}(t)$ may be seen as an analytic function and can be approximated through a simplified Taylor expansion determined at $(t = 0)$:

$$\tilde{y}(t) \simeq y(t) = \sum_{j=0}^{n}\frac{y^{(j)}(0)}{j!}t^j \tag{19}$$

This identifying technique includes many algebraic manipulations of the functional domain with the same principles as Laplace transformation. The underlying expression is eventually translated into time domain and can be found in the following steps:

1. Define the noisy signal's first-order approximation $\tilde{y}(t)$ around $t = 0$:

$$y(t) = a_0 + a_1 t \tag{20}$$

2. Applying the Laplace transformation known rules and Cauchy formula, after some mathematical rearrangement:

$$\frac{Y(s)}{s^2} + \frac{1}{s}\frac{d}{ds}Y(s) = -\frac{a_1}{s^4} \tag{21}$$

3. The resulted time domain first-order derivative estimation is the following:

$$\dot{y} = a_1 = -\frac{6}{t^3}\int_0^t (t-2\tau)y(\tau)\mathrm{d}\tau \tag{22}$$

4. The unknown function F_{approx} can be identified then by the derivative estimator (Der) in real-time using (23):

$$F_{\text{approx}} = \dot{y} - \beta u(t) = -\frac{6}{t^3}\int_0^t ((t-2\tau)y(\tau) - \beta u(t))\mathrm{d}\tau \tag{23}$$

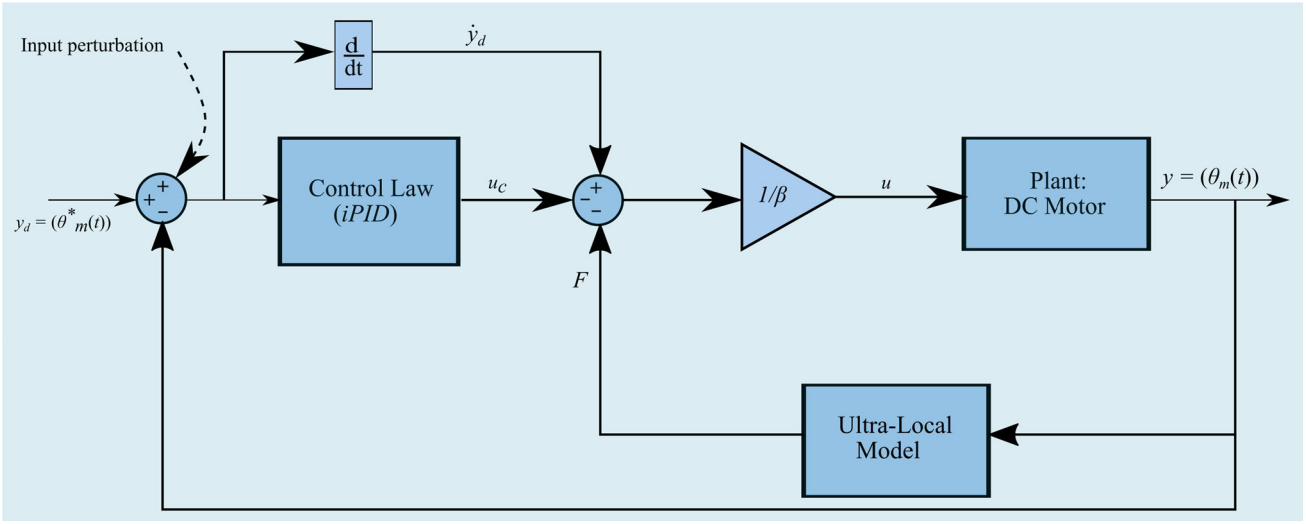

Fig. 1 MFC scheme

5 Discrete Implementation of the Ultra-local Model

The above expressions (18) and (23) of the estimated parameter F will be digitally implemented using an FIR filter. For other implementations using ALIEN filters, see (Fliess and Sira-Ramirez 2003).

5.1 Discrete Implementation of the Derivative Estimator (Der)

Consider again the noisy signal $\tilde{y}(t)$ described in (19), the approximation is relevant for ϵ at a short interval and can be represented as follows:

$$\dot{y} \simeq \dot{y}(0) = a_1 = \frac{k}{q(t)} \int_0^t \tilde{Q}(t,\tau) y(\tau) \mathrm{d}\tau; 0 < t < \epsilon \quad (24)$$

and implemented in a short time with a fixed-length window T:

$$\dot{y} = \frac{k}{q(T)} \int_0^T \tilde{Q}(T,\tau) y(\tau) \mathrm{d}\tau = \int_0^T \frac{k\tilde{Q}(T,\tau)}{q(T)} y(\tau) \mathrm{d}\tau = \int_0^T Q(T,\tau) y(\tau) \mathrm{d}\tau \quad (25)$$

The description above presents an estimation of the functional $\dot{y} = a_1$ that exists only in the neighborhood of $t = 0$, as this approximation is based on the expansion of Taylor series around $t = 0$. Typically, the approximation is appropriate if the signal is a polynomial without noise. The evaluation drifts over time for an arbitrary signal. The reason for this is basically $a_1 = \dot{y}(0)$ should be equivalent to $a_1 = \dot{y}(t)$ in order to approximate the derivative at $t = 0$ in a short time $0 < t < \epsilon$. Conversely, the estimator is not causal: $y(t)$ for $t > 0$ then, it allows the signal values to be estimated at $t = 0$. This inspires the modification of the system to create at time t a causal estimator where the coefficients can be determined through the estimators introduced by the following steps:

1. Assume the Taylor expansion $x(\tau)$ near $\tau = 0$ of the signal $\tilde{x}(\tau)$:

$$\tilde{x}(\tau) \simeq x(\tau) = \sum_{j=0}^{n} a_1 \tau \Rightarrow a_1 = \int_0^T Q(T,\tau) x(\tau) \mathrm{d}\tau \quad (26)$$

2. By changing the variables $\tau \triangleq t - \theta$ and $y(\theta) \triangleq x(t-\theta)$:

$$y(\theta) \triangleq x(t-\theta) = \sum_{j=0}^{n} a_1 (t-\theta) \quad (27)$$

This expression can be considered as a Taylor expansion $\tilde{x}(\tau)$ for $\theta = t$ with a reversal signal for the parameter θ:

$$\dot{y}(t) = \frac{d}{d\theta}(x(t-\theta))\Big|_{\theta=t} = (-1)a_1 \quad (28)$$

3. Again by changing the variable a_1:

$$a_1 = \int_0^T Q(T,\tau) x(\tau) \mathrm{d}\tau = \int_0^T Q(T,\tau) y(t-\tau) \mathrm{d}\tau \quad (29)$$

A causal estimator is determined using a specified estimation window of length T at time t:

$$\dot{y}(t) = a_1 = (-1)\int_0^T Q(T,\tau)y(t-\tau)\mathrm{d}\tau \tag{30}$$

A digital FIR Filter is feasible to implement the above estimator through a trapezoidal integration procedure. In this context, we consider $T = T_s N$, where T is the estimation window, T_s is the fixed sampling time, and $(N+1)$ is the number of samples:

$$\dot{y}(t) = a_1 \simeq (-1)\sum_{k=1}^{N+1} \alpha_k Q\left(T,\tau_k\right) y\left(t-\tau_k\right) \tag{31}$$

The discretion of $Q\left(T,\tau_k\right)$ is theoretically estimated to reduce the computational cost, where we also consider the coefficients (α_k) obtained from the integration of trapezoids:

$$\begin{aligned}
&\hat{Q}_{\alpha_k}\left(T,\tau_k\right) = \\
&\quad\left[\alpha_1 Q\left(T,\tau_1\right)\alpha_2 Q\left(T,\tau_2\right)\ldots\alpha_{N+1} Q\left(T,\tau_{N+1}\right)\right] \\
&\tau_k = (k-1)T_s \\
&\alpha_k = \frac{T_s}{2}, k = 1 \text{ or } k = N+1 \\
&\alpha_k = T_s, k = 2,3,\ldots,N
\end{aligned} \tag{32}$$

The buffer array $\hat{y}\left(t-\tau k\right)$ that includes the last samples of $(N+1)$ is ordered vertically, and the whole vector is relocated for each sample clock. The very last value is discounted, and the newest value of $y(t)$ is pushed to the first place:

$$\hat{y}\left(t-\tau_k\right) = \begin{bmatrix} y(t) \\ y\left(t-T_s\right) \\ \vdots \\ y\left(t-T_s N\right) \end{bmatrix} \tag{33}$$

Eventually, for each sample time, $\hat{Q}\alpha_k\left(T,\tau_k\right)$ and $\hat{y}\left(t-\tau_k\right)$ are multiplied, ensuring an online update estimation of $\dot{y}$:

$$\begin{aligned}
\dot{y}(t) = a_1(t) &\simeq (-1)\sum_{k=1}^{N+1} \alpha_k Q\left(T,\tau_k\right) y\left(t-\tau_k\right) \\
&= (-1)\hat{Q}_{\alpha_k}\left(T,\tau_k\right)\hat{y}\left(t-\tau_k\right)
\end{aligned} \tag{34}$$

It is necessary to note that a distinction between noise and accuracy is defined by the estimating window T. Although smaller values of T have a quick filter response and better contextual signal modeling, larger values increase noise sensitivity with higher frequency filtering characteristics. Given that the filter coefficients may be high (particularly for high order estimators), the window should be large enough to minimize the inherent numerical error to the discrete expression in (31). The sampling frequency may also be increased ordinarily if the hardware operates at the highest level of numerical accuracy.

Given that today, the computational effort is not constrained because we now have access to quick and low-cost micro-controllers. These filters are being effectively implemented simultaneously. However, the complexity of computation gradually increases with the number of samples, as $(N+1)$ multiplication and (N) sums are necessary to make the approximation at each time step.

Finally, after the estimation of $\dot{y}$ and back to equation (23) using the last control input to measure the actual parameter, F can be determined using the following equation:

$$\widehat{F}_k = \dot{y}_k - \beta u_{k-1} \tag{35}$$

5.2 Discrete Implementation of the Algebraic Estimator (Alg)

Consider again the estimation expression of the parameter F presented in (18). An FIR filter is suitable for digital implementation. The previous approach has been revised, and we incorporate the restricted fixed-length window T backward to achieve a feasible online implementation relative to the estimator described in Sect. 5.1. In this case, F is calculated as an independent time constant, so it does not modify that signal in the reverse integration. After some change of variables, equation (36) is the final expression for the algebraic estimator of F(Alg).

After certain variables have changed, F represented in (18) is finally the following:

$$F = \frac{-6}{T^3}\int_0^T (t-2\tau)y(t-\tau)d\tau - \frac{6\beta}{T^3}\int_0^T \tau(T-\tau)u(t-\tau)d\tau \tag{36}$$

An appropriate selection of any variable means that the computed discrete filter parameters are stored in a vector (considering trapezoidal integration coefficients). For the estimation of the current control input in (12), the previous value of the control input is used to prevent an algebraic loop. Thus, the identification of F is constant, and no further problem in this method even though the approximation is taken in a small sliding window T.

6 Controller Design

The present section describes the used feedback control method for the resolution of the position tracking of the DC motor. The execution of model-free control laws is significantly affected by the parameters β and iPD/iPID gains.

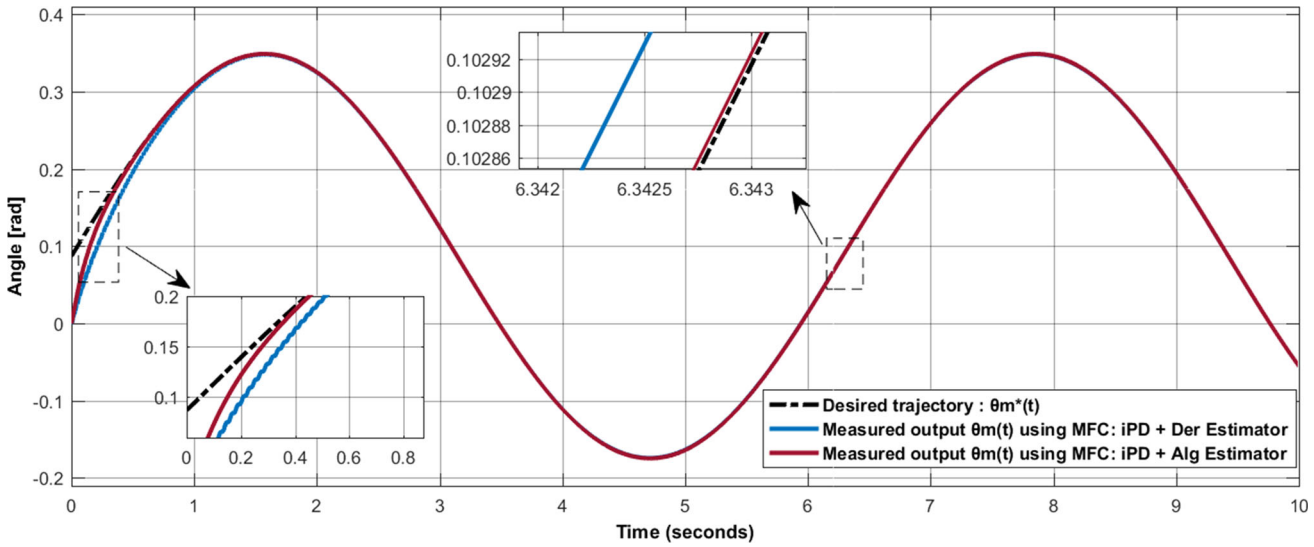

Fig. 2 Sinusoidal trajectory—Position tracking of the DC motor in the presence of Coulombs friction effects using ultra-local model based on algebraic and derivative estimators

Therefore, for better performance, a tuning procedure is presented in Sects. 6.1 and 6.2, respectively.

6.1 Tuning Procedure of the iPD/iPID Gains

An iPD and iPID controllers are used in the coming simulations, suppose again $v = 1$ in (6):

$$F(t) = \dot{y}(t) - \beta u(t) \tag{37}$$

As in Fig. 1, the loop is closed with an intelligent Proportional-Integral-Derivative (iPID) controller:

$$u = \frac{-F + y_d - K_I \int e - K_P e - K_D \dot{e}}{\beta} \tag{38}$$

where y_d is the reference trajectory, $e = y_d - y$ is the tracking error, and $\{K_P, K_I, K_D\}$ are the frequent PID tuning gains.

For an iPD controller, selecting $K_P = \lambda^2$, $K_I = 0$, and $K_D = 2\lambda, \lambda \in \mathbb{R}^+$ provides a stable closed loop of two real negative poles equivalent to $-\lambda$ (Laid and Boubekeur 2020):

$$\ddot{e} + \lambda^2 e + 2\lambda \dot{e} = 0 \tag{39}$$

For an iPID controller, selecting $K_P = 3\lambda^2$, $K_I = \lambda^3$, and $K_D = 3\lambda, \lambda \in \mathbb{R}^+$ provides a stable closed loop loop of three real negative poles equivalent to $-\lambda$ (Laid and Boubekeur 2020):

$$\ddot{e} + \lambda^3 \int e + 3\lambda^2 e + 3\lambda \dot{e} = 0 \tag{40}$$

6.2 Tunning Procedure of β

Consider the current output signal dynamics described in (6) in the following form:

$$\dot{y} = \widetilde{F}(t) + \widetilde{\beta}(t) u \tag{41}$$

where $\widetilde{F}(t)$ and $\widetilde{\beta}(t)$ refer to two unspecified time functions, this is now:

$$F = \widetilde{F}(t) + (\widetilde{\beta}(t) - \beta) u \tag{42}$$

$$u = -\left(\frac{\widehat{F} - \dot{y}_d}{\beta}\right) - \mathcal{Q}(e) \tag{43}$$

where $\mathcal{Q}(e)$ represents the tracking error correction.

By integrating (41) in (43) and choosing $\mathcal{Q}(e)$ to be equal to 0, i.e., taking account of just feed-forward expression of the control law, that refers to:

$$\dot{y} = \frac{\widetilde{\beta}(t)}{\beta} \dot{y}_d + \left(\widetilde{F}(t) - \frac{\widetilde{\beta}(t)}{\beta} \widehat{F}\right) \tag{44}$$

The measurement of $\hat{F}$ is sensitive to particular dynamics, as the controller's performance is essentially determined by the estimation error $|\widehat{F} - F|$. Thus, the value of β must be specially picked as similar to the actual system gain to avoid significant changes of F.

For $\beta \to +\infty$, the control signal u demonstrated in (43) is referred to $\mathcal{Q}(e)$. In that case, the controller is simplified to a classic PID controller.

For $\beta \to 0^+$, the control signal u becomes mainly based on the estimation $\widehat{F}$. Thus, β is easily tuned just by setting $\mathcal{Q}(e) = 0$ and observing various values of β. First choose

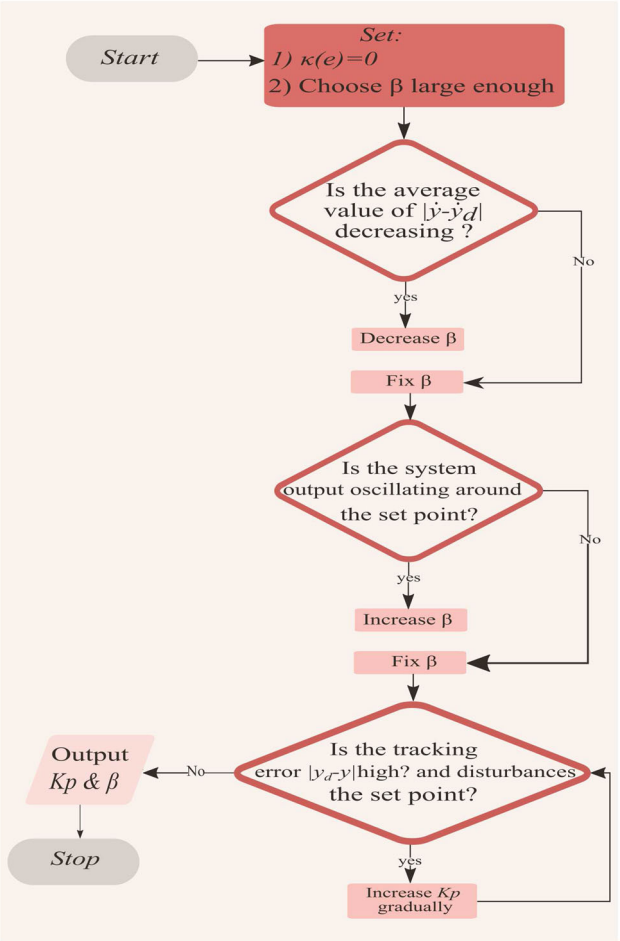

Fig. 3 Tuning protocol of the parameter β

β high enough, the control signal is approximately zero. Second, reducing the value of β will rise the control signal average until the reference closed-loop condition is satisfied ($\dot{y} = \dot{y}_d$). Figure 3 summarizes the tuning procedure of β.

7 Simulations Results

Numerical simulations were conducted to confirm the efficiency of the implemented control law with regard to fast convergence of the tracking error into a limited region of zero, low control effort and smooth transient responses for an inaccurate expertise input perturbation of the effect caused by Coulomb friction or noisy measurements that affect the system.

The controller gains are chosen by placing the closed-loop poles in a proper position on the real negative axis. In this study, the poles have been placed at $p = -100$ rad/s, and the values of the PD and PID gains $\{K_P, K_I, K_D\}$ were determined by the expressions described in (39) and (40).

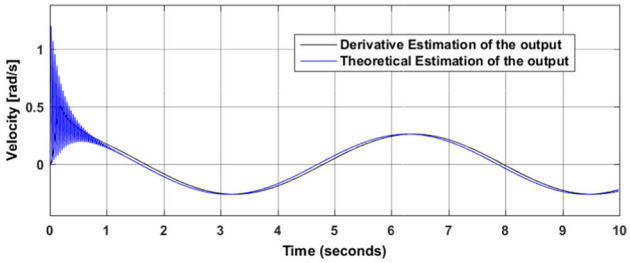

Fig. 4 Sinusoidal trajectory—Derivative estimation of the angular velocity $\hat{\dot{y}} = (\hat{\dot{\theta}}_m(t))$

The efficiency of the model-free control approach implemented using the ultra-local model based on algebraic/derivative estimators is shown by two distinct trajectories:

1. A sinusoidal position tracking such that, $\theta_m^* = A\ \sin(\omega t) + B$ with an amplitude $A = \pi/12$ (rad), a bias $B = \pi/36$ (rad) and a frequency $\omega = 1$ (rad/s).
2. A nominal trajectory defined through an eight order Bezier's polynomial, which interpolates smoothly from 0 to 1 at the interval of time $[t_i, t_f]$.

$$\theta_m^*(t) = \theta_m^*(t_i) + (\theta_m^*(t_f) - \theta_m^*(t_i))\varphi\left(\tau, t_f, t_i\right) \qquad (45)$$

where $\tau = (t - t_i) / \left(t_f - t_i\right)$.

The study was carried out with a sampling frequency of 10kHz. In both approaches of algebraic and derivative estimation of F in (35) and (36), an estimation window of $T = 0.2s$, a fixed sampling time of T_s=0.0001s, and a number of samples $N = 2000$ were used.

In the following simulations, "Der" denotes the estimation of the parameter F in (5) through angular velocity, "Alg" denotes the algebraic estimation of F in (36), and the measured output {y}, the reference input $\{y_d\}$, the control signal $\{u\}$ will be used to refer to: $\{\theta_m(t)\}$, $\{\theta_m^*(t)\}$, $\{V\}$, respectively. The first-order derivative of the output $\dot{y}$ used in (23) is estimated through a derivative estimator and compared with a theoretical derivator (see Fig. 4). For each estimation method, different values of β were set to provide a good response as described in Fig. 3. The tuning procedure proposed in Sect. 6.2 was used to apply the ultra-local model-based estimators control law. It simply takes a few minutes to fine-tune the controller. To proceed, the proportional gain K_P is considered to be zero. Then, a reference trajectory is provided once the plant is at rest, and open-loop system responses for various values of β are collected. Beginning with $\beta_{Alg} = 1000$, $\beta_{Der} = 1000$ and reducing their values until the control signal attempts to oscillate at $\beta_{Alg} = 1$, $\beta_{Der} = 45$. Afterward, The proportional gain K_P is adjusted so that the tracking error is reasonable. Finally, β_{Alg} and β_{Der} are set to 3 and 100 respectively.

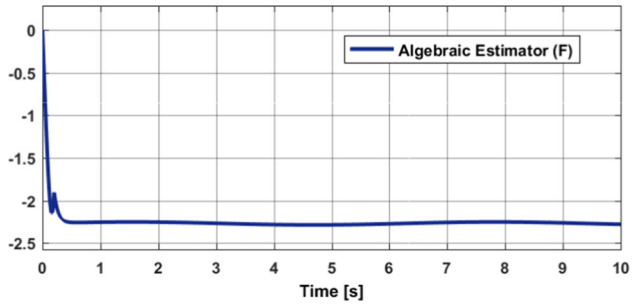

Fig. 5 Sinusoidal trajectory—Algebraic estimation of the unmodeled dynamics

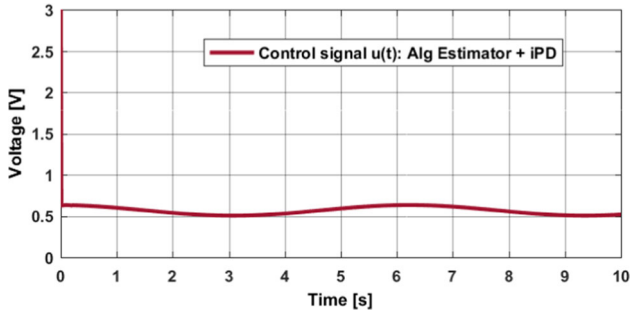

Fig. 6 Sinusoidal trajectory—Control signal effort for the algebraic estimator with iPD

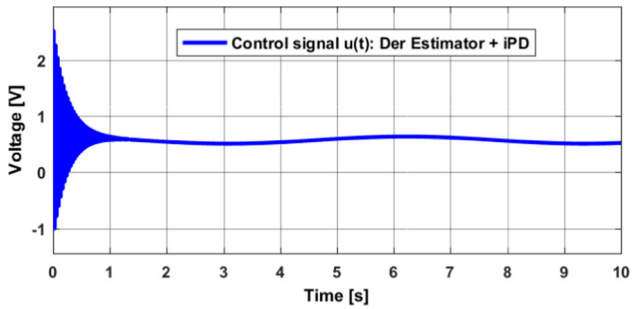

Fig. 7 Sinusoidal trajectory—Control signal effort for the derivative estimator with iPD controllers

Figure 2 illustrates the numerical results of the proposed controllers where the main purpose is to maintain a desired sinusoidal output position in the presence of the previously mentioned causes of uncertainties. At time $t = 0.01$ s, the estimation of the function F and the angular velocity start the online update as illustrated in Figs. 4 and 5, with a voltage control effort signal presented in Figs. 6 and 7, respectively, in order to cancel the perturbations resulting from Coulomb friction effects.

Figure 8 shows the position tracking error using the two proposed controllers based on algebraic and derivative estimators. The feedback controller adjusts the DC motor's position, drives the state errors to a relatively short time frame of zero, and regulates for the model parameters' errors.

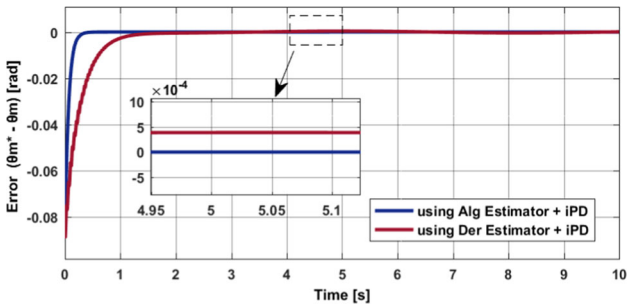

Fig. 8 Sinusoidal trajectory—Tracking error evolution using algebraic/derivative estimators with iPD

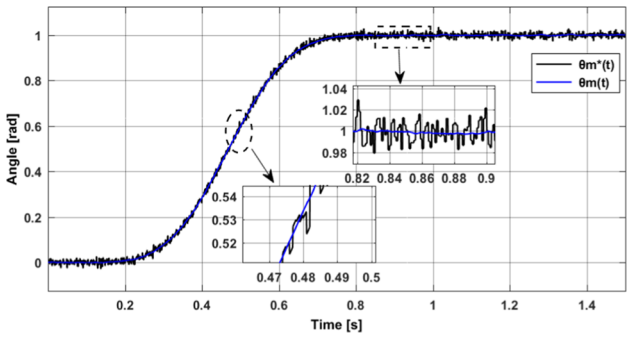

Fig. 9 Perturbed Bezier's trajectory—Position tracking of the DC motor in the presence of Coulomb's friction effects using algebraic estimator with iPID

Table 2 Sinusoidal trajectory–Effectiveness of the control techniques based on ISE, IAE and ITAE criterions

Control technique	ISE	IAE	ITAE
iPD + Derivative Estimator	0.12×10^{-2}	0.03	0.03
iPD + Algebraic Estimator	0.48×10^{-3}	0.01	0.002
Classical PD	0.4×10^{-2}	0.19	0.96

Table 3 Perturbed Bezier's trajectory—Effectiveness of the control techniques based on ISE, IAE and ITAE criterions

Control technique	ISE	IAE	ITAE
iPD + Derivative Estimator	0.41×10^{-2}	0.09	0.21
iPD + Algebraic Estimator	0.1×10^{-2}	0.08	0.19
Classical PID	0.86×10^{-2}	0.26	0.47

The research results show an excellent model-free control tracking efficiency, which is easily better tracked when an integral factor is included. In the derivative scheme, the control signal was noisier, and the system less robust. Increasing the estimation window can increase the filtering characteristics, but the resulting delay may cause the closed-loop to be unstable.

In Figs. 9 and 10, we set an eighth order Bezier's polynomial input disturbance signal that is large enough for the

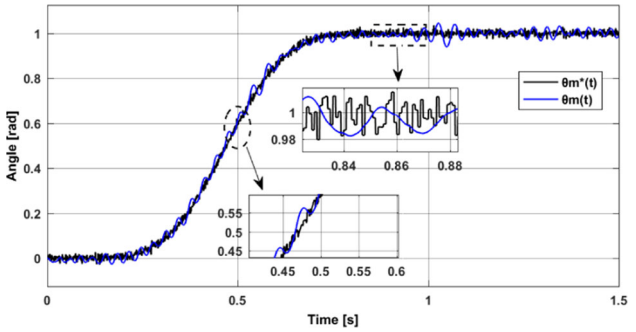

Fig. 10 Perturbed Bezier's trajectory—Position tracking of the DC motor in the presence of Coulomb's friction effects using derivative estimator with iPID

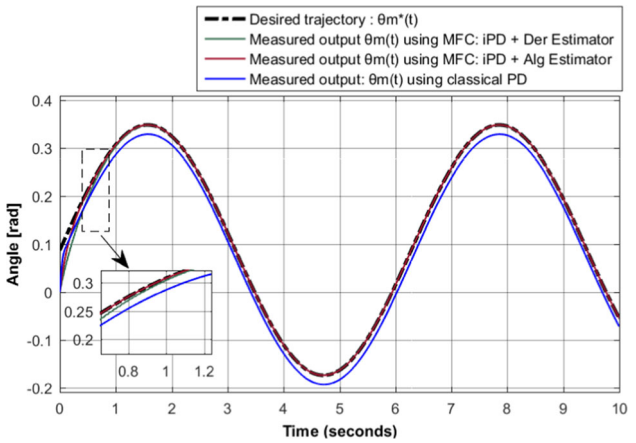

Fig. 11 Sinusoidal trajectory—Comparison between algebraic/derivative estimators with iPD and classical PD

system to deform the input signal to evaluate the controller's smoothing efficiency for the cases of algebraic and derivative estimators.

Furthermore, the performance of the control approaches has been analyzed according to the integral time absolute tracking error, $ITAE = \int_{t_i}^{t_f} t \left| e_{\theta_m}(t) \right| \mathrm{d}t$, the integral absolute tracking error, $IAE = \int_{t_i}^{t_f} \left| e_{\theta_m}(t) \right| \mathrm{d}t$, and the integral squared tracking error, $ISE = \int_{t_i}^{t_f} e_{\theta_m}^2(t) \mathrm{d}t$, in which $t_i = 0$ s and $t_f = 10$ s denote the simulation's initial and final times. The ISE and IAE standards classify all tracking errors uniformly. Moreover, since time is a significant consideration in the ITAE standard, errors that eventuate slowly are highly penalized, while errors that arise slightly earlier are ignored. Tables 1 and 2 compare the obtained results, illustrating that the proposed control of the ultra-local model based on algebraic estimator slight performs better than the model based on derivative estimator.

Finally, the proposed ultra-local model-based algebraic/derivative estimator approaches are compared to a classical PID, which is among the most widely used controllers. A classical PD is used for the sinusoidal trajectory, and a classical PID is used for the perturbed Bezier's trajectory.

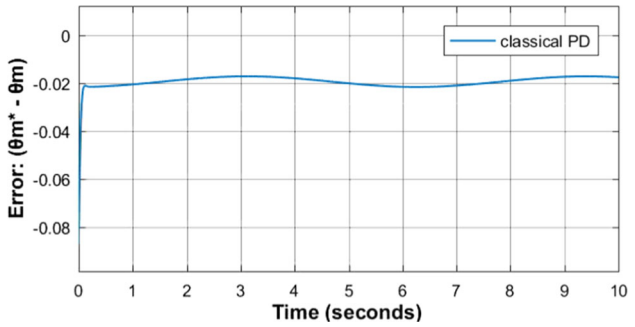

Fig. 12 Sinusoidal trajectory—Tracking error evolution using classical PD

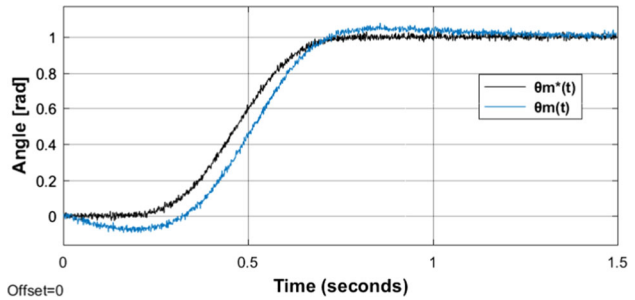

Fig. 13 Perturbed Bezier's trajectory—Position tracking of the DC motor in the presence of Coulomb's friction effects using classical PID

The PD/PID controllers were hand-tuned to achieve a quick closed-loop response with minimal overshoots across the desired trajectory.

Figures 11 and 12 depict the obtained results. In the transient region, the iPD controllers track the desired trajectory faster than the classical PD controller. This is attributed to the control law's factor $\dot{y}_d$, see Eq. (7). Moreover, the proposed approaches provided accurate robust tracking results with regard to the Coulomb friction disturbances. It can be seen from Figs. 9, 10 and 13 that iPIDs for the case of algebraic and derivative estimators strongly cancel the perturbations and provide smooth Bezier trajectory. At $t = 0.25$ s, the PID controller reveals an overshoot that can be minimized at the tradeoff of slow tracking. A comparison in terms of ISE, IAE and ITAE criterions is highlighted in Tables 2 and 3. The other potential problem with the classical PID is how to provide an appropriate adaptability as the plant changes over time; this can be solved using the proposed ultra-local model based on algebraic and derivative estimators.

8 Conclusion

This work discussed model-free controllers' design based on the ultra-local model combined with algebraic and derivative estimators and their application on a DC motor position track-

ing. Particularly, different necessary implementing details including the discrete implementation of the estimators and the control law parameters' tuning procedure are demonstrated and successfully implemented using FIR filters.

Simulation results show that the ultra-local model's implementation via derivative estimation is feasible and reliable when used as an observer in closed-loop control, but the algebraic estimation still gives better results. All the presented controllers had an excellent robust tracking performance regarding the Coulomb friction disturbances and uncertainties and compared to the classical PID.

The proposed algebraic and derivative estimation techniques are significant since they are based exclusively on algebra, preventing a nonlinear observer, complex mathematical modeling tasks, and providing a fast and accurate estimation.

The main flaw in the algebraic/derivative estimators lies with the need for a high-frequency sampler and the assertion that the computing effort is increased following the filter's length and is limited to fast hardware applications. Interestingly, it is not a challenge, as powerful hardware is currently available and relatively inexpensive.

A further research incorporates a fractional-order study of the ultra-model's output for $0 < v < 1$. Besides that, the proposed approaches should be also tested on different other models.

Declarations

Conflict of interest The authors declare that they have no conflict of interest.

References

Aravind, M. A., Saikumar, N., & Dinesh, N. S. (2017). Optimal position control of a dc motor using lqg with ekf. In *2017 International conference on mechanical, system and control engineering (ICMSC)* (pp. 149–154).

Barth, J. M., Condomines, J.-P., Moschetta, J.-M., Cabarbaye, A., Join, C., & Fliess, M. (2019). Full model-free control architecture for hybrid uavs. In *2019 American control conference (ACC)* (pp. 71–78). IEEE.

Bembli, S., Haddad, N. K., & Belghith, S. (2021). A robust model free terminal sliding mode with gravity compensation control of a 2 dof exoskeleton-upper limb system. *Journal of Control, Automation and Electrical Systems, 32*(3), 632–641.

Bhushan, B., & Singh, M. (2011). Adaptive control of dc motor using bacterial foraging algorithm. *Applied Soft Computing, 11*(8), 4913–4920.

Eker, I. (2004). Open-loop and closed-loop experimental on-line identification of a three-mass electromechanical system. *Mechatronics, 14*(5), 549–565.

Eker, I. (2006). Sliding mode control with pid sliding surface and experimental application to an electromechanical plant. *ISA Transactions, 45*(1), 109–118.

Fliess, M., & Join, C. (2013). Model-free control. *International Journal of Control, 86*(12), 2228–2252.

Fliess, M., Join, C., & Sira-Ramirez, H. (2008). Non-linear estimation is easy. *International Journal of Modelling, Identification and Control, 4*(1), 12–27.

Fliess, M., & Sira-Ramirez, H. (2003). An algebraic framework for linear identification. ESAIM: Control. *Optimisation and Calculus of Variations, 9,* 151–168.

Glida, H. E., Abdou, L., Chelihi, A., Sentouh, C., et al. (2020). Optimal model-free backstepping control for a quadrotor helicopter. *Nonlinear Dynamics, 100*(4), 3449–3468.

Guermouche, M., Ali, S. A., & Langlois, N. (2015). Super-twisting algorithm for dc motor position control via disturbance observer. *IFAC-PapersOnLine, 48*(30), 43–48.

Laid, S. & Boubekeur, B. (2020). Model-free and adaptive control of a dc motor: A comparative study. In *2020 international conference on electrical engineering (ICEE)* (pp. 1–6). IEEE.

Lyshevski, S. E. (1999). Nonlinear control of mechatronic systems with permanent-magnet DC motors. *Mechatronics, 9*(5), 539–552.

Mahfouf, M., Kee, C., Abbod, M. F., & Linkens, D. A. (2000). Fuzzy logic-based anti-sway control design for overhead cranes. *Neural Computing & Applications, 9*(1), 38–43.

Mamani, G., Becedas, J., Feliu-Batlle, V., & Sira-Ramirez, H. (2007). Open-loop algebraic identification method for a dc motor. In *2007 European Control Conference (ECC)*, pages 3430–3436. IEEE.

Mamani, G., Becedas, J., Feliu-Batlle, V., & Sira-Ramírez, H. (2009). Open-and closed-loop algebraic identification method for adaptive control of DC motors. *International Journal of Adaptive Control and Signal Processing, 23*(12), 1097–1103.

Mboup, M., Join, C., & Fliess, M. (2007). A revised look at numerical differentiation with an application to nonlinear feedback control. In *2007 mediterranean conference on control and automation* (pp. 1–6). IEEE.

Moraes, M. S. & da Silva, P. S. P. (2015). Model-free control of magnetic levitation systems through algebraic derivative estimation. In *Proceedings of 23rd ABCM international congress of mechanical engineering, Rio de Janeiro*.

Mummadi, V. C. (2000). Steady-state and dynamic performance analysis of pv supplied dc motors fed from intermediate power converter. *Solar Energy Materials and Solar Cells, 61*(4), 365–381.

Mungporn, P., Yodwong, B., Thounthong, P., Nahid-Mobarakeh, B., Takorabet, N., Guilbert, D., Kumam, P., Bizon, N., & Kaewprapha, C. (2019). Model-free control of multiphase interleaved boost converter for fuel cell/reformer power generation. In *2019 research, invention, and innovation congress (RI2C)* (pp. 1–6). IEEE.

Nouri, K., Dhaouadi, R., & Braiek, N. B. (2008). Adaptive control of a nonlinear dc motor drive using recurrent neural networks. *Applied Soft Computing, 8*(1), 371–382.

Olsson, H., Åström, K. J., De Wit, C. C., Gäfvert, M., & Lischinsky, P. (1998). Friction models and friction compensation. *Eur. J. Control 4*(3), 176–195.

Polack, P., Delprat, S., & d'Andréa Novel, B. (2019). Brake and velocity model-free control on an actual vehicle. *Control Engineering Practice 92*, 104072.

Ruderman, M., Iwasaki, M., & Chen, W.-H. (2020). Motion-control techniques of today and tomorrow: A review and discussion of the challenges of controlled motion. *IEEE Industrial Electronics Magazine, 14*(1), 41–55.

Tang, C. P., Miller, P. T., Krovi, V. N., Ryu, J.-C., & Agrawal, S. K. (2010). Differential-flatness-based planning and control of a wheeled mobile manipulator-theory and experiment. *IEEE/ASME Transactions on Mechatronics, 16*(4), 768–773.

Wang, F., Zhao, X., Zhang, D., Ma, Z., & Jing, X. (2011). Robust and precision control for a directly-driven xy table. *Proceedings of the Institution of Mechanical Engineers, Part C: Journal of Mechanical Engineering Science, 225*(5), 1107–1120.

Yavin, Y. (2007). Control of the motion of a disk rolling on a plane curve. *Computers & Mathematics with Applications, 54*(11–12), 1329–1340.